

# THE LICK AGN MONITORING PROJECT 2011: REVERBERATION MAPPING OF MARKARIAN 50

AARON J. BARTH<sup>1</sup>, ANNA PANCOAST<sup>2</sup>, SHAWN J. THORMAN<sup>1</sup>, VARDHA N. BENNETT<sup>2,3</sup>, DAVID J. SAND<sup>2,4</sup>, WEIDONG LI<sup>5</sup>, GABRIELA CANALIZO<sup>6</sup>, ALEXEI V. FILIPPENKO<sup>5</sup>, ELINOR L. GATES<sup>7</sup>, JENNY E. GREENE<sup>8</sup>, MATTHEW A. MALKAN<sup>9</sup>, DANIEL STERN<sup>10</sup>, TOMMASO TREU<sup>2</sup>, JONG-HAK WOO<sup>11</sup>, ROBERTO J. ASSEF<sup>10,12</sup>, HYUN-JIN BAE<sup>13</sup>, BRENDON J. BREWER<sup>2</sup>, TABITHA BUEHLER<sup>14</sup>, S. BRADLEY CENKO<sup>5</sup>, KELSEY I. CLUBB<sup>5</sup>, MICHAEL C. COOPER<sup>1,15</sup>, ALEKSANDAR M. DIAMOND-STANIC<sup>16,17</sup>, KYLE D. HINER<sup>6</sup>, SEBASTIAN F. HÖNIG<sup>2</sup>, MICHAEL D. JONER<sup>14</sup>, MICHAEL T. KANDRASHOFF<sup>5</sup>, C. DAVID LANEY<sup>14</sup>, MARIANA S. LAZAROVA<sup>6</sup>, A. M. NIERENBERG<sup>2</sup>, DAWOO PARK<sup>11</sup>, JEFFREY M. SILVERMAN<sup>5,18</sup>, DONGHOON SON<sup>11</sup>, ALESSANDRO SONNENFELD<sup>2</sup>, ERIK J. TOLLERUD<sup>1</sup>, JONELLE L. WALSH<sup>1,19</sup>, RICHARD WALTERS<sup>20</sup>, ROBERT L. DA SILVA<sup>21</sup>, MICHELE FUMAGALLI<sup>21</sup>, MICHAEL D. GREGG<sup>22</sup>, CHELSEA E. HARRIS<sup>2</sup>, ERIC Y. HSIAO<sup>18</sup>, JEFFREY LEE<sup>17</sup>, LILIANA LOPEZ<sup>17</sup>, JACOB REX<sup>5</sup>, NAO SUZUKI<sup>18</sup>, JONATHAN R. TRUMP<sup>21</sup>, DAVID TYTLER<sup>17</sup>, GÁBOR WORSECK<sup>21</sup>, AND HASSEN M. YESUF<sup>21</sup>

*Draft version February 18, 2022*

## ABSTRACT

The Lick AGN Monitoring Project 2011 observing campaign was carried out over the course of 11 weeks in Spring 2011. Here we present the first results from this program, a measurement of the broad-line reverberation lag in the Seyfert 1 galaxy Mrk 50. Combining our data with supplemental observations obtained prior to the start of the main observing campaign, our dataset covers a total duration of 4.5 months. During this time, Mrk 50 was highly variable, exhibiting a maximum variability amplitude of a factor of  $\sim 4$  in the  $U$ -band continuum and a factor of  $\sim 2$  in the  $H\beta$  line. Using standard cross-correlation techniques, we find that  $H\beta$  and  $H\gamma$  lag the  $V$ -band continuum by  $\tau_{\text{cen}} = 10.64^{+0.82}_{-0.93}$  and  $8.43^{+1.30}_{-1.28}$  days, respectively, while the lag of He II  $\lambda 4686$  is unresolved. The  $H\beta$  line exhibits a symmetric velocity-resolved reverberation signature with shorter lags in the high-velocity wings than in the line core, consistent with an origin in a broad-line region dominated by orbital motion rather than infall or outflow. Assuming a virial normalization factor of  $f = 5.25$ , the virial estimate of the black hole mass is  $(3.2 \pm 0.5) \times 10^7 M_{\odot}$ . These observations demonstrate that Mrk 50 is among the most promising nearby active galaxies for detailed investigations of broad-line region structure and dynamics.

*Subject headings:* galaxies: active — galaxies: individual (Mrk 50) — galaxies: nuclei

<sup>1</sup> Department of Physics and Astronomy, 4129 Frederick Reines Hall, University of California, Irvine, CA, 92697-4575, USA; barth@uci.edu

<sup>2</sup> Department of Physics, University of California, Santa Barbara, CA 93106, USA

<sup>3</sup> Physics Department, California Polytechnic State University, San Luis Obispo, CA 93407, USA

<sup>4</sup> Las Cumbres Observatory Global Telescope Network, 6740 Cortona Drive, Suite 102, Santa Barbara, CA 93117, USA

<sup>5</sup> Department of Astronomy, University of California, Berkeley, CA 94720-3411, USA

<sup>6</sup> Department of Physics and Astronomy, University of California, Riverside, CA 92521, USA

<sup>7</sup> Lick Observatory, P. O. Box 85, Mount Hamilton, CA 95140, USA

<sup>8</sup> Department of Astrophysical Sciences, Princeton University, Princeton, NJ 08544, USA

<sup>9</sup> Department of Physics and Astronomy, University of California, Los Angeles, CA 90095-1547, USA

<sup>10</sup> Jet Propulsion Laboratory, California Institute of Technology, 4800 Oak Grove Boulevard, Pasadena, CA 91109, USA

<sup>11</sup> Astronomy Program, Department of Physics and Astronomy, Seoul National University, Seoul 151-742, Republic of Korea

<sup>12</sup> NASA Postdoctoral Program Fellow

<sup>13</sup> Department of Astronomy and Center for Galaxy Evolution Research, Yonsei University, Seoul 120-749, Republic of Korea

<sup>14</sup> Department of Physics and Astronomy, N283 ESC, Brigham Young University, Provo, UT 84602-4360, USA

<sup>15</sup> Hubble Fellow

<sup>16</sup> Southern California Center for Galaxy Evolution Fellow

<sup>17</sup> Center for Astrophysics and Space Sciences, University of California, San Diego, CA 92093-0424, USA

<sup>18</sup> Physics Division, Lawrence Berkeley National Laboratory, 1 Cyclotron Road, Berkeley, CA 94720, USA

<sup>19</sup> Department of Astronomy, The University of Texas at Austin, Austin, TX 78712, USA

<sup>20</sup> Caltech Optical Observatories, California Institute of Technology, Pasadena, CA 91125, USA

<sup>21</sup> Department of Astronomy and Astrophysics, UCO/Lick Observatory,

University of California, 1156 High Street, Santa Cruz, CA 95064, USA

<sup>22</sup> Department of Physics, University of California Davis, Davis, CA 95616, USA; IGPP, Lawrence Livermore National Laboratory, Livermore, CA 94550, USA

## 1. INTRODUCTION

Observations of broad-line variability in nearby Seyfert galaxies play a central role in the interpretation of the demographics and cosmological evolution of supermassive black holes in active galactic nuclei (AGNs). By measuring the time delay between AGN continuum variations and the subsequent response of the broad-line region (BLR) gas, the light-travel time across the BLR, and hence the mean BLR radius ( $r_{\text{BLR}}$ ), can be directly measured. These reverberation-mapping measurements have been carried out for a few dozen low-redshift AGNs (e.g., Kaspi et al. 2000; Peterson et al. 2004; Bentz et al. 2009a), and the observed BLR sizes measured via  $H\beta$  reverberation range from typically a few light-days up to several light-months. The BLR size is observed to scale with AGN continuum luminosity roughly as  $r_{\text{BLR}} \propto L^{0.5}$  (Bentz et al. 2009b), and this relationship makes it possible to estimate BLR radii from a single observation of an AGN.

With a direct measurement or estimate of  $r_{\text{BLR}}$ , and assuming virial motion of BLR clouds, it becomes possible to estimate the mass of the black hole in an AGN as  $M_{\text{BH}} = fr_{\text{BLR}}(\Delta V)^2/G$ , where  $\Delta V$  is the width of the broad line, and  $f$  is a dimensionless scaling factor (e.g., Ulrich et al. 1984; Kaspi et al. 2000; Onken et al. 2004). This method has been used to estimate black hole masses in large samples of AGNs out to the highest observed redshifts (for a review, see Vestergaard 2011). Currently, nearly all observational constraints on the cosmological growth history of supermassive black holes depend on masses derived from this virial equation. While the assumption of virial motion in the BLR has gained support from a variety of consistency checks (e.g., Peterson & Wandel 2000; Onken et al. 2004; Nelson et al. 2004), it remains extremely difficult to obtain direct constraints on the structure and dynamical state of the BLR in any individual AGN, and in the absence of such constraints, the inferred black hole masses remain subject to substantial systematic uncertainty (Krolik 2001). The most promising method to examine the kinematics of BLR gas is velocity-resolved reverberation mapping, in which the time-delay response of emission-line variability relative to continuum fluctuations can be measured as a function of line-of-sight velocity. Velocity-resolved reverberation data can encode a wealth of information about BLR structure on spatial scales that are orders of magnitude too small to be resolved by any other technique (e.g., Welsh & Horne 1991; Horne et al. 2004).

Recently, high-cadence observing campaigns have produced major improvements in the quality of velocity-resolved reverberation data for the broad Balmer lines (Bentz et al. 2009a; Denney et al. 2010). For the most highly variable objects, it is possible to examine the shape of the two-dimensional transfer function, which describes the distribution of broad-line lag response time as a function of velocity (Bentz et al. 2010), and to apply new modeling techniques that can directly constrain the BLR geometry and potentially test the critical assumption of virial motion (Pancoast et al. 2011a; Brewer et al. 2011). In order to increase the number of objects with data suitable for such analysis, we carried out a new reverberation-mapping campaign in Spring 2011.

In this *Letter*, we present our first results for Mrk 50, a Seyfert 1 galaxy at redshift  $z = 0.023$ . Past observations have found dramatic variations in its nuclear luminosity (Pastoriza et al. 1991), but it has not previously been a reverberation-mapping target. During our monitoring pro-

gram, Mrk 50 exhibited strong variability, and we detect a robust reverberation signal and a significant velocity-resolved reverberation response across the broad  $H\beta$  emission line.

## 2. OBSERVATIONS AND REDUCTIONS

## 2.1. Photometry

From 2011 January 21 until June 13 (all dates are UT), we obtained queue-scheduled  $V$ -band images using the 0.76 m Katzman Automatic Imaging Telescope at Lick Observatory (Filippenko et al. 2001), the 0.9 m telescope at the Brigham Young West Mountain Observatory (WMO), the Super-LOTIS 0.6 m telescope at Kitt Peak, the Faulkes Telescope South at Siding Spring Observatory, and the Palomar 1.5 m telescope (Cenko et al. 2006). Exposure times were typically 180–300 s. We attempted to observe Mrk 50 on a nightly basis, but poor weather and telescope scheduling issues left some gaps in temporal coverage.

All images were bias-subtracted and flattened, and cosmic-ray hits were removed using the LA-COSMIC routine (van Dokkum 2001). In order to remove the host galaxy and obtain a light curve of the variable AGN flux, we employed image subtraction using the HOTPANTS package by A. Becker<sup>23</sup>, which is based on the algorithm described by Alard (2000). For each telescope, a high-quality template image was chosen, and the template was then aligned with each night's image and convolved with a spatially varying kernel to match the point-spread function of that image. After subtracting the scaled template image, the variable AGN flux is left as a point source in the subtracted image, allowing for aperture photometry using the IRAF DAOPHOT package. The photometric aperture radius used for each telescope was set to match the average point-source full width at half-maximum intensity (FWHM) for images from that telescope. Light curves were constructed separately for each telescope, and each was then normalized to the WMO light curve by determining an average flux scaling factor based on nights when Mrk 50 was observed at both locations. We find that the image subtraction yields a better-quality light curve than simple aperture photometry, and provides closer agreement between the light curves obtained with different telescopes.

The overall flux scale was calibrated using observations of Landolt (1992) standard stars observed during a few photometric nights at WMO. Observations taken within 6 hr of one another were combined by taking a weighted average. The final  $V$  light curve is illustrated in Figure 1.

## 2.2. Spectroscopy

Our campaign at the Lick Shane 3 m telescope consisted of 69 nights allocated between 2011 March 27 and June 13, during which time we observed Mrk 50 on 41 nights using the Kast dual spectrograph (Miller & Stone 1993). In this paper, we discuss only measurements from the blue arm of the spectrograph, where we used a 600 lines  $\text{mm}^{-1}$  grism over  $\sim 3440\text{--}5520 \text{ \AA}$  at a scale of  $1.0 \text{ \AA pixel}^{-1}$ . All observations were done with a  $4''$ -wide slit oriented at  $PA = 180^\circ$ . Standard calibration frames including arc lamps and dome flats were observed each afternoon, and flux standards were observed during twilight. The exposure time for Mrk 50 was normally  $2 \times 1200 \text{ s}$ . Additionally, we observed Mrk 50 on 18 nights that were allocated to other observing programs, beginning on January 26. All observations used the same 600-line grism

<sup>23</sup> [http://www.astro.washington.edu/users/becker/c\\_software.html](http://www.astro.washington.edu/users/becker/c_software.html)

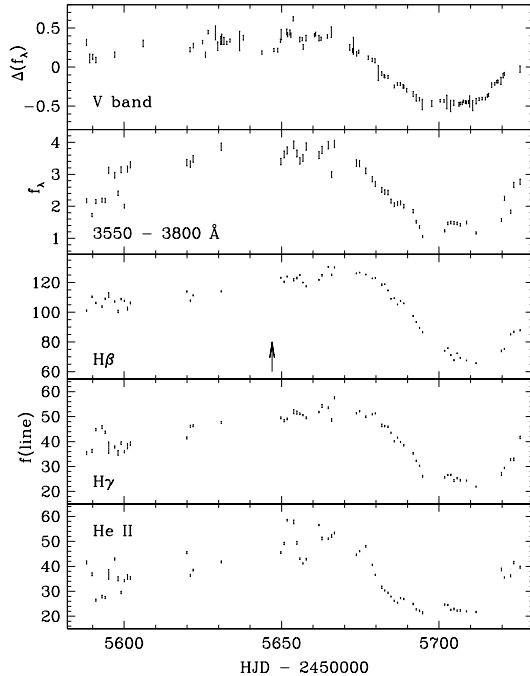


FIG. 1.— Mrk 50 light curves for the V band, the  $U_s$ -band continuum measured from the spectra over 3550–3800 Å, and the H $\beta$ , H $\gamma$ , and He II emission lines. The V-band panel shows a difference imaging light curve illustrating changes in flux relative to the mean. Units for the V and  $U_s$  bands are  $10^{-15}$  erg cm $^{-2}$  s $^{-1}$  Å $^{-1}$ , and units for broad-line fluxes are  $10^{-15}$  erg cm $^{-2}$  s $^{-1}$ . The arrow in the H $\beta$  light curve marks the start of the dedicated Lick observing campaign.

and 4'' slit, but the wavelength coverage was slightly different each time. The exposure for these observations was typically 900 s.

Spectroscopic reductions and calibrations followed standard methods implemented in IRAF and IDL. A large extraction width of 10.''3 was used in order to accommodate the full extent of the AGN spatial profiles observed on nights with very poor seeing. Error spectra were extracted and propagated through the full sequence of calibrations, and for each night the two exposures of Mrk 50 were averaged together. In the region 4600–4800 Å, the median signal-to-noise ratio per pixel is 75.

### 3. SPECTROSCOPIC DATA ANALYSIS

The reduced spectra were first normalized to a uniform flux scale by employing the procedure of van Groningen & Wanders (1992). This method applies a flux scaling factor, a linear wavelength shift, and a Gaussian convolution to each spectrum in order to minimize the residuals between the data and a reference spectrum constructed from several of the best-quality nights. The scaling is determined using a wavelength range containing the [O III]  $\lambda$ 5007 line, which is assumed to have constant flux.

Since the spectra contain a substantial amount of host-galaxy starlight, we implemented a simple continuum subtraction routine to produce a cleaner measurement of the broad-line profiles and fluxes, similar to the procedure described by Park et al. (2011). Over the wavelength range 4300–5400 Å, each scaled spectrum was fitted with a model consisting of a power-law featureless continuum, an Fe II tem-

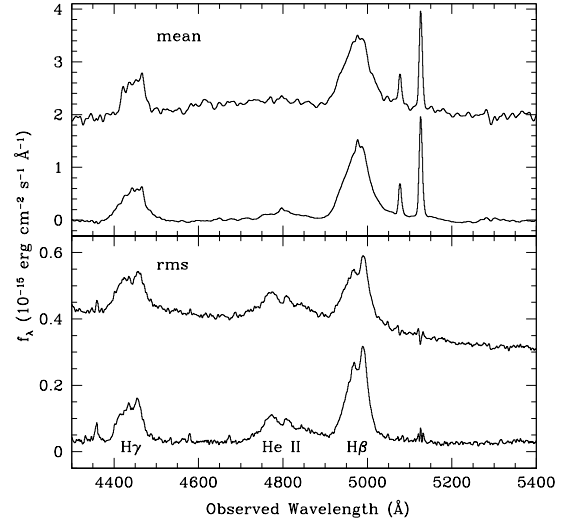


FIG. 2.— Mean and rms spectra. In each panel, the upper spectrum is constructed from the set of scaled spectra of Mrk 50, and the lower spectrum is constructed from the continuum-subtracted, scaled spectra.

plate from Boroson & Green (1992) broadened by convolution with a Gaussian kernel, several emission-line components represented by either Gaussians or Gauss-Hermite functions (van der Marel & Franx 1993), and a starlight model consisting of simple stellar population models at solar metallicity from Bruzual & Charlot (2003) which were broadened by convolution with a Gaussian kernel. Additionally, a foreground extinction was applied to the model spectrum. The model fit was optimized by  $\chi^2$  minimization using a Levenberg-Marquardt technique (Markwardt 2009). Then, the best-fitting model components representing the starlight and nonstellar continuum were subtracted from the data, leaving a pure emission-line spectrum. For the starlight model, we obtained a good fit using an 11 Gyr-old population as the dominant component, and adding contributions from younger populations did not significantly improve the fit. The median starlight fraction at  $\lambda_{\text{rest}} = 5100$  Å is 41%, and Fe II contributes just  $\sim 2$ –3% of the continuum flux density at 4600 Å.

In prior reverberation work, starlight subtraction has not generally been applied, and the broad-line light curves have typically been measured by subtracting a local, linear continuum fitted to wavelength regions on either side of an emission line. We find that our continuum subtraction procedure provides a more accurate removal of the continuum shape underlying each emission line and a much better light curve for the weak He II  $\lambda$ 4686 line. Figure 2 shows two versions of the mean and root-mean-square (rms) spectra: one constructed from the set of scaled spectra, and one constructed from the set of continuum-subtracted, scaled spectra. This illustrates the utility of the continuum subtraction procedure for removing the stellar absorption features and continuum undulations.

The broad-line light curves were then measured by integrating the flux over fixed wavelength ranges in the continuum-subtracted spectra: 4890–5050 Å for H $\beta$ , 4370–4510 Å for H $\gamma$  (also including the narrow [O III]  $\lambda$ 4363 line), and 4730–4870 Å for He II. Emission-line light curves are shown in Figure 1, along with the continuum flux density measured from the scaled spectra over 3550–3800 Å (which we refer to as the  $U_s$  band). The continuum and broad lines were highly variable during the monitoring period: over a 30-day span the  $U_s$ -band

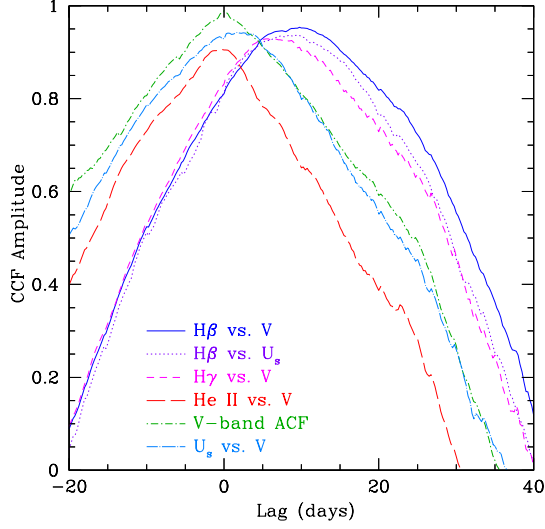


FIG. 3.— Cross-correlation functions for  $H\beta$ ,  $H\gamma$ , and He II against the AGN continuum flux, the autocorrelation function of the V-band continuum, and the cross-correlation of the continuum bands  $U_s$  vs. V.

continuum dropped by a factor of  $\sim 4$ , and the  $H\beta$  line responded with a factor of  $\sim 2$  decline. For observations taken before the start of our dedicated campaign on March 27, the scatter in the spectroscopic light curves is relatively high. We attribute this to the nightly differences in observational setup and calibrations used by each observing team, and to the very poor observing conditions during some winter nights.

To estimate black hole masses from reverberation data, the second moment of the  $H\beta$  line in the rms spectrum is most often used as the measure of line width (Peterson et al. 2004). We find  $\sigma(H\beta_{\text{rms}}) = 1740 \pm 101 \text{ km s}^{-1}$ , where the measurement uncertainty is determined through a bootstrap resampling procedure (Bentz et al. 2009a), and the line width has been corrected for instrumental broadening of  $\sigma_{\text{inst}} \approx 133 \text{ km s}^{-1}$  following Barth et al. (2011).

#### 4. REVERBERATION LAG MEASUREMENTS

In order to measure the cross-correlation function (CCF) for unevenly sampled time series, we employ the interpolation cross-correlation function methodology and Monte Carlo error analysis techniques described by Gaskell & Peterson (1987), White & Peterson (1994), and Peterson et al. (2004); these methods have been employed in the majority of recent reverberation-mapping work (e.g., Bentz et al. 2009a; Denney et al. 2010). We measured the cross-correlations of  $H\beta$ ,  $H\gamma$ , and He II against the V light curve, and also of  $H\beta$  against the  $U_s$  light curve. The CCFs were computed from  $-20$  to  $+40$  days in increments of 0.25 days. Table 1 lists two measures of the lag:  $\tau_{\text{peak}}$ , which is the lag at the peak of the CCF, and  $\tau_{\text{cen}}$ , the centroid of the CCF for all points above 80% of the peak value (Peterson et al. 2004). Figure 3 illustrates the CCF measurements.

The  $H\beta$  and  $H\gamma$  lines have similar lag times of  $\tau_{\text{cen}} = 10.64$  and 8.43 days, respectively, but for He II we find that both  $\tau_{\text{cen}}$  and  $\tau_{\text{peak}}$  are consistent with zero lag, indicating a very compact size for the inner, high-ionization portion of the BLR. The faster response time for He II is apparent in the light curves, particularly in the steep drop beginning in mid-April (HJD  $\approx 2455670$ ). The Balmer lines, in contrast, show a much more gradual and delayed decline in response to the falling continuum flux. The flattened peak and asymmetry

TABLE 1  
CROSS-CORRELATION LAG RESULTS

Measurement	$\tau_{\text{cen}}$ (days)	$\tau_{\text{peak}}$ (days)
$H\beta$ vs. V	$10.64^{+0.82}_{-0.93}$	$9.75^{+0.50}_{-1.00}$
$H\gamma$ vs. V	$8.43^{+1.30}_{-1.28}$	$7.00^{+1.75}_{-1.50}$
He II vs. V	$-0.97^{+1.18}_{-1.07}$	$-0.25^{+0.75}_{-1.25}$
$H\beta$ vs. $U_s$	$9.58^{+1.05}_{-0.90}$	$8.75^{+1.00}_{-1.25}$
$U_s$ vs. V	$0.60^{+1.26}_{-1.19}$	$1.25^{+1.50}_{-1.00}$

NOTE. — All lags are given in the observed frame.

of the  $H\beta$  CCF in comparison with the continuum autocorrelation function (ACF) suggests that the Balmer-line emitting zone of the BLR covers a fairly large radial extent, and this interpretation is supported by the velocity-resolved measurements described below. We also measured the CCF between the  $U_s$  and V bands in order to search for evidence of reverberation due to Balmer continuum emission from the BLR (Maoz et al. 1993; Korista & Goad 2001), but no significant lag was found.

Our Mrk 50 dataset, which benefits from high-amplitude variability and high-cadence sampling, presents an excellent case study for velocity-resolved variability. Light curves were measured for seven separate velocity segments across the width of the  $H\beta$  line, and each segment light curve was cross-correlated against the V light curve. Figure 4 illustrates the lag ( $\tau_{\text{cen}}$ ) as a function of velocity across the  $H\beta$  line, revealing a roughly symmetric trend of shorter lags in the line wings and longer lags in the core, with a  $\sim 10$  day difference in response time between the core and wings. This pattern, which resembles the symmetric  $H\beta$  lag response seen in some other AGNs including Mrk 110 (Kollatschny & Bischoff 2002) and NGC 5548 (Denney et al. 2010), is qualitatively consistent with predictions for BLR clouds in circular orbits in the Keplerian potential of the black hole (e.g., Welsh & Horne 1991), with the highest line-of-sight velocities originating from gas located close to the black hole. In contrast, a BLR dominated by either radial infall or outflow would result in an asymmetric velocity-lag map, with inflow producing longer lags on the blueshifted side of the line, and outflow producing longer lags on the red side. Such signatures of radial motion have been seen in a few objects (Bentz et al. 2009a; Denney et al. 2010), but the current sample of AGNs with velocity-resolved data of this quality is still too small to examine the distribution of different BLR kinematic states.

#### 5. BLACK HOLE MASS ESTIMATE

Following Peterson et al. (2004), we compute the  $H\beta$  “virial product” [defined as  $\text{VP} = r_{\text{BLR}}(\Delta V)^2/G$ ] by using  $\Delta V = \sigma(H\beta_{\text{rms}})$  and  $r_{\text{BLR}} = c\tau_{\text{cen}}$ , where  $\tau_{\text{cen}}$  has been corrected to the AGN rest frame. For Mrk 50,  $r_{\text{BLR}} = 10.40^{+0.80}_{-0.91}$  lt-days, and  $\text{VP} = (6.2 \pm 0.9) \times 10^6 M_{\odot}$ .

While the virial product is a straightforward combination of measured quantities, the relationship between virial product and black hole mass is more indirect and uncertain. Most recent reverberation work has adopted a normalization of the virial mass scale based on the assumption that AGNs as a whole fall on the same  $M_{\text{BH}} - \sigma$  relation as nearby inactive galaxies (Onken et al. 2004; Woo et al. 2010). Using the  $M_{\text{BH}} - \sigma$  relation derived by Gültekin et al. (2009) as the local reference, this implies a mean value of  $\log f = 0.72^{+0.09}_{-0.10}$ , and the reverberation masses determined in this way show an intrinsic scatter of 0.44 dex about the  $M_{\text{BH}} - \sigma$  relation

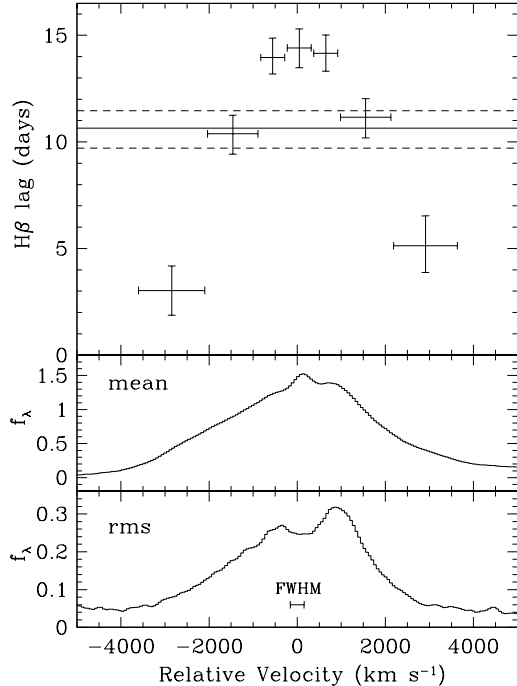


FIG. 4.— Velocity-resolved reverberation in the  $H\beta$  line. The upper panel shows the mean lag measured for each velocity segment of the broad  $H\beta$  line, with the horizontal error bar representing the width of the velocity segment. The overall lag for  $H\beta$  and its uncertainty range are shown by solid and dashed lines. The lower panels show the mean and rms continuum-subtracted spectra, and the error bar indicates the FWHM due to instrumental broadening.

(Woo et al. 2010). Adopting the Woo et al. value of  $f = 5.25$  implies that  $M_{\text{BH}} = (3.2 \pm 0.5) \times 10^7 M_{\odot}$  for Mrk 50. For consistency with recent work (Peterson et al. 2004; Bentz et al. 2009a; Denney et al. 2010), the quoted uncertainty includes only the statistical error on the virial product, but not the uncertainty resulting from the choice of a specific  $f$  value; the true uncertainty in  $M_{\text{BH}}$  is dominated by the uncertainty in  $f$ . Masses derived in this way depend on the assumption of virial motion, the assumption that AGNs should fall on the same  $M_{\text{BH}} - \sigma$  relation as quiescent galaxies, and the adoption of a specific  $M_{\text{BH}} - \sigma$  relation as the local baseline. Differing assessments of the form of the local  $M_{\text{BH}} - \sigma$  relation, particularly at low masses, can potentially affect the normalization of the AGN virial mass scale at the factor of  $\sim 2$  level (Greene et al. 2010; Graham et al. 2011). Additionally, there is ongoing debate over the possible effect of radiation pressure on BLR clouds and its impact on the inferred masses (Marconi et al. 2008; Netzer & Marziani 2010). Thus, while the mean value of  $f$  can currently be determined to  $\sim 20\%$  precision within the context of a specific set of assumptions about the  $M_{\text{BH}} - \sigma$  relation (Woo et al. 2010; Graham et al. 2011), the actual uncertainty in the overall AGN mass scale

remains significantly larger and is difficult to quantify, and the observed 0.44 dex scatter in the AGN  $M_{\text{BH}} - \sigma$  relation must reflect, at least in part, the dispersion of the true  $f$  values for individual AGNs. Resolving these issues will require enlarging the number of targets having high-quality reverberation-mapping data, and the application of new approaches to extract dynamical information from the observations (e.g., Pancoast et al. 2011a; Brewer et al. 2011).

Mrk 50 has an early-type morphology, and Malkan et al. (1998) classify it as an S0 galaxy based on *Hubble Space Telescope* imaging. The only published measurement of the stellar velocity dispersion of Mrk 50 is  $\sigma_{\star} = 78 \pm 15 \text{ km s}^{-1}$  based on a Sloan Digital Sky Survey spectrum (Greene & Ho 2006). However, a new measurement from Keck LRIS data gives  $109 \pm 14 \text{ km s}^{-1}$  (Harris et al., in preparation), and we consider this to be more reliable than the SDSS measurement. The scaling relations calibrated by Gültekin et al. (2009) then imply an expected  $M_{\text{BH}} \approx (0.6 - 1.7) \times 10^7 M_{\odot}$  from the general  $M_{\text{BH}} - \sigma$  relation including ellipticals and spirals, or  $(0.9 - 2.5) \times 10^7 M_{\odot}$  based on the  $M_{\text{BH}} - \sigma$  relation fitted to ellipticals only. Our reverberation-based mass is slightly higher than these values, but Mrk 50 still lies well within the  $\sim 0.4$  dex scatter of the AGN  $M_{\text{BH}} - \sigma$  relation (Woo et al. 2010).

## 6. CONCLUSIONS AND FUTURE WORK

From our Spring 2011 monitoring campaign, we have obtained very high-quality reverberation mapping of Mrk 50. This is one of just a few nearby AGNs in which strong velocity-resolved lag signatures have been detected, and it is now among the most promising targets for detailed studies of BLR geometry and kinematics.

Our long observing campaign produced a large and very rich dataset, and this paper presents just one set of early results from this program. Future papers will include detailed descriptions of the data-analysis procedures and results for the entire observed sample. A major goal of our project is to exploit the potential of velocity-resolved reverberation mapping to elucidate the structure of the BLR and to derive black hole masses directly, and an upcoming paper (Pancoast et al. 2011b) will describe new modeling of our Mrk 50 data. The black hole mass determined from dynamical modeling is consistent with the simple virial estimate presented here, and Mrk 50 is now the second object (after Arp 151; Brewer et al. 2011) to show agreement between the two approaches.

We are extremely grateful to the Lick Observatory staff for their outstanding support during our observing run. The Lick AGN Monitoring Project 2011 is supported by NSF grants AST-1107812, 1107865, 1108665, and 1108835. T.T. acknowledges a Packard Research Fellowship. The West Mountain Observatory receives support from NSF grant AST-0618209. We thank Brad Peterson for a helpful referee report.

*Facilities:* Shane (Kast), KAIT, BYU:0.9m, PO:1.5m, LCOGT (FTS), Super-LOTIS

## REFERENCES

- Alard, C. 2000, *A&AS*, 144, 363
- Barth, A. J., et al. 2011, *ApJ*, 732, 121
- Bentz, M. C., et al. 2009a, *ApJ*, 705, 199
- Bentz, M. C., Peterson, B. M., Netzer, H., Pogge, R. W., & Vestergaard, M. 2009b, *ApJ*, 697, 160
- Bentz, M. C., et al. 2010, *ApJ*, 720, L46
- Boroson, T. A., & Green, R. F. 1992, *ApJS*, 80, 109
- Brewer, B. J., et al. 2011, *ApJ*, 733, L33
- Bruzual, G., & Charlot, S. 2003, *MNRAS*, 344, 1000
- Cenko, S. B., et al. 2006, *PASP*, 118, 1396
- Denney, K. D., et al. 2010, *ApJ*, 721, 715
- Filippenko, A. V., Li, W. D., Treffers, R. R., & Modjaz, M. 2001, in *Small Telescope Astronomy on Global Scales*, ed. W. P. Chen, et al. (San Francisco: ASP), 121
- Gaskell, C. M., & Peterson, B. M. 1987, *ApJS*, 65, 1

- Graham, A. W., Onken, C. A., Athanassoula, E., & Combes, F. 2011, *MNRAS*, 412, 2211
- Greene, J. E., & Ho, L. C. 2006, *ApJ*, 641, L21
- Greene, J. E., et al. 2010, *ApJ*, 721, 26
- Gültekin, K., et al. 2009, *ApJ*, 698, 198
- Horne, K., Peterson, B. M., Collier, S. J., & Netzer, H. 2004, *PASP*, 116, 465
- Kaspi, S., Smith, P. S., Netzer, H., Maoz, D., Jannuzi, B. T., & Giveon, U. 2000, *ApJ*, 533, 631
- Kollatschny, W., & Bischoff, K. 2002, *A&A*, 386, L19
- Korista, K. T., & Goad, M. R. 2001, *ApJ*, 553, 695
- Krolik, J. H. 2001, *ApJ*, 551, 72
- Landolt, A. U. 1992, *AJ*, 104, 340
- Malkan, M. A., Gorjian, V., & Tam, R. 1998, *ApJS*, 117, 25
- Maoz, D., et al. 1993, *ApJ*, 404, 576
- Marconi, A., Axon, D. J., Maiolino, R., Nagao, T., Pastorini, G., Pietrini, P., Robinson, A., & Torricelli, G. 2008, *ApJ*, 678, 693
- Markwardt, C. B. 2009, *Astronomical Data Analysis Software and Systems XVIII*, 411, 251
- Miller, J. S., & Stone, R. P. S. 1993, *Lick Obs. Tech. Rep.* 66 (Santa Cruz, CA: Lick Observatory)
- Nelson, C. H., Green, R. F., Bower, G., Gebhardt, K., & Weistrop, D. 2004, *ApJ*, 615, 652
- Netzer, H., & Marziani, P. 2010, *ApJ*, 724, 318
- Onken, C. A., Ferrarese, L., Merritt, D., Peterson, B. M., Pogge, R. W., Vestergaard, M., & Wandel, A. 2004, *ApJ*, 615, 645
- Pancoast, A., Brewer, B. J., & Treu, T. 2011a, *ApJ*, 730, 139
- Pancoast, A., et al. 2011b, submitted
- Park, D., et al. 2011, *ApJ*, submitted
- Pastoriza, M. G., Bica, E., Bonatto, C., Mediavilla, E., & Perez, E. 1991, *AJ*, 102, 1696
- Peterson, B. M., & Wandel, A. 2000, *ApJ*, 540, L13
- Peterson, B. M., et al. 2004, *ApJ*, 613, 682
- Ulrich, M. H., et al. 1984, *MNRAS*, 206, 221
- van der Marel, R. P., & Franx, M. 1993, *ApJ*, 407, 525
- van Dokkum, P. G. 2001, *PASP*, 113, 1420
- van Groningen, E., & Wanders, I. 1992, *PASP*, 104, 700
- Vestergaard, M. 2011, in *Black Holes*, ed. M. Livio & A. M. Koekemoer (Cambridge: Cambridge Univ. Press), 150
- Welsh, W. F., & Horne, K. 1991, *ApJ*, 379, 586
- White, R. J., & Peterson, B. M. 1994, *PASP*, 106, 879
- Woo, J.-H., et al. 2010, *ApJ*, 716, 269